European Journal of Medicinal Chemistry 146 (2018) 501–510

Contents lists available at ScienceDirect

European Journal of Medicinal Chemistry

journal homepage: http://www.elsevier.com/locate/ejmech

Research paper

Novel vitexin-inspired scaffold against leukemia

Taotao Ling, Walter Lang, Xiang Feng, Sourav Das, Julie Maier, Cynthia Jeffries, Anang Shelat, Fatima Rivas*

Department of Chemical Biology and Therapeutics, St. Jude Children's Research Hospital, Memphis, TN 38105-3678, USA

ARTICLE INFO

Article history:
Received 23 June 2017
Received in revised form
4 December 2017
Accepted 1 January 2018

Keywords:
Vitexin
Quinolin-4(1H)-one
Cdk inhibitor
Reactive oxygen species

ABSTRACT

Acute lymphoblastic leukemia (ALL) is the most common type of leukemia in children. Up to a quarter of ALL patients relapse and face poor prognosis. To identify new compound leads, we conducted a phenotypic screen using terrestrial natural product (NP) fractions against immortalized ALL cellular models.

We identified vitexin, a flavonoid, as a promising hit with biological activity ($EC_{50} = 30\ \mu M$) in pre-B cell ALL models with no toxicity against normal human tissue (BJ cells) at the tested concentrations. To develop more potent compounds against ALL and elucidate its potential mode of action, a vitexin-inspired compound library was synthesized. Thus, we developed an improved and scalable protocol for the direct synthesis of 4-quinolone core heterocycles containing an *N*-sulfonamide using a one-pot condensation reaction protocol. The newly generated compounds represent a novel molecular scaffold against ALL as exemplified by compounds **13** and **15**, which demonstrated EC_{50} values in the low micromolar range (0.3–10 μM) with little to no toxicity in normal cellular models. Computational studies support the hypothesis that these compounds are potential CDK inhibitors. The compounds induced apoptosis, caused cell arrest at G0/G1 and G2/M, and induced ROS in cancer cells.

1. Introduction

Acute lymphoblastic leukemia (ALL) is the most common type of leukemia in children [1]. Up to a quarter of ALL patients relapse and face poor prognosis [2]. Relapsed ALL cases are associated with initial poor response and chemotherapy resistance [1–4]. New potent compounds are required to effectively treat relapsed ALL. Our drug discovery program objective is to identify new chemical scaffolds to advance the bench-to-bedside therapeutic agent development process in high-risk and drug-resistant leukemia.

Based on a phenotypic screen using stable B cellular ALL models (representatives of this high-risk patient cohort), we expected to identify specific molecular scaffolds to expand our knowledge on current treatment modalities against ALL. We identified the natural product vitexin (**1**, Fig. 1) as a hit compound. Vitexin has been isolated from several sources including *Acer palmatum* [5]. Vitexin was reported as a potent hypotensive inhibitor of ganglion activity, with anti-inflammatory, *anti*-histamic, anti-cancer and anti-bradykinin among a broad range of other biological activities including antioxidant properties [5–7]. Some glycosylated flavonoids have a direct bond between the sugar and the anomeric carbon (O-C bond), while others such as vitexin feature the sugar bond at C6 or C8 (C-C bond). Studies of natural products have led to the development of clinical candidates such as flavopiridol (*Alvocidib*, **4**, with FDA orphan drug designation to treat AML, Fig. 1), flavonoid-like and FDA approved ATP-mimetic compound **5** (Fig. 1) [8]. Mechanistic studies of flavonoid compounds suggest a two-prone mode of action, CDK inhibition (particularly CDK9) and various cellular effects from metabolic changes to antioxidant activity [8]. Recently, the treatment of chronic lymphocytic leukemia by flavopiridol in clinical trials was successfully reported [9]. Compounds **4** and **5** were used as control compounds in this study.

The antioxidant activity of flavonoids depends on the molecular structure, the degree of hydroxylation/glycosylation, and the positions of hydroxyl groups as they provide resonance effects on the aromatic ring for radical atom engagement. Some of the most widely studied isoflavones are genistein (**2**, Fig. 1) and baicalein (**3**, Fig. 1), which reacts with topoisomerase II via radical mechanism, disrupting the maintenance of DNA stability, and wogonin induces autophagy [10]. However, their biological effects are observed in

* Corresponding author. Department of Chemical Biology and Therapeutics, St. Jude Children's Research Hospital, 262 Danny Thomas Place, Memphis, TN 38105-3678, USA.
E-mail address: Fatima.rivas@stjude.org (F. Rivas).

https://doi.org/10.1016/j.ejmech.2018.01.004
0223-5234/

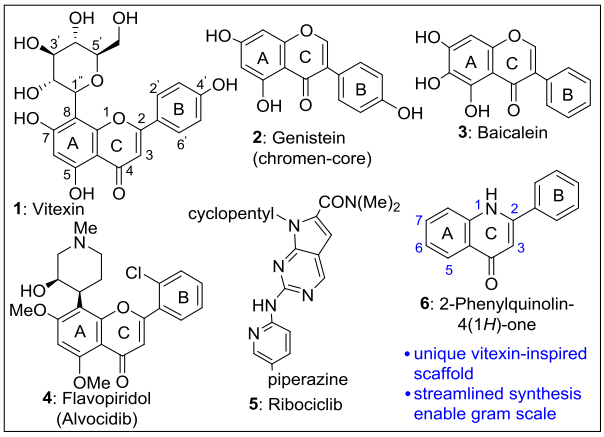

Fig. 1. Vitexin and related molecular scaffolds.

the high micromolar range as solubility/cellular permeability are some of the obstacles for the chromen core compounds [6]. While natural products (NPs) show potent bioactivities, their modest bioavailability properties can be affected by the presence and number of hydrophilic moieties (i.e. sugars, which can modulate water solubility and cell permeability). Thus, the introduction of heteroatoms and polar functional groups could lead to modified NPs with improved bioavailability properties.

The lack of scaffold diversity among standard care agents against leukemia and relapsed patients strongly supports the investigation of new chemical matter. We developed a vitexin-inspired library based on the hypothesis that a quinolone core (**6**, Fig. 1) instead of the chromen core (**2**, Fig. 1) would display improved biological activity against ALL since such compounds would a) decrease overall electronegativity due to the nitrogen, b) enable hydrogen bonding via donor rather than acceptor, and c) provide a handle to introduce functional groups to survey the chemical space. Thus, the resulting compounds would be more potent than vitexin, potentially enabling the development of a new class of chemical agents against high-risk and relapsed ALL.

Our studies describe an efficient synthesis, structure-activity relationship (SAR) studies of quinolin-4(1H)-one derivatives inspired by vitexin against ALL cellular models and the potential biological target(s).

2. Results and discussion

The study began by developing suitable synthetic conditions to generate the core synthons required for biological evaluation. On the basis of their chemical structures, the quinolone derivatives were divided into 3 group series (Scheme 1). Series I consisted of derivatives with 2-(4-methoxyphenyl) quinolone and 6, 8-dimethoxy on the A ring to explore the biological effect of the *N*-1 substituents and potentially improve biological potency. Series II derivatives focused on the role of C2 substituents via amide formation and evaluation of the electronic effects of these substituents. Series III included the evaluation of C6 to explore alternative functional groups to the methoxy groups and reduce potential metabolic liabilities, while maintaining biological activity. Thus, the combined group series would enable the generation of the corresponding *N*-sulfonamides, 2-amino-benzenethiazoles connected at C2 and urea moiety at C6 for a thorough biological evaluation.

Synthetic methodologies to access 4-quinolone derivatives are frequently based on intramolecular cyclization reactions mediated by acid or base (i.e. Conrad-Limpach or Gould-Jacobs reactions). Once we identified 3, 5-dimethoxy aniline and 4-nitroaniline as the synthetic building blocks for our 4-quinolone libraries, reaction conditions were evaluated to access the desired core compounds [11a]. Nucleophilic addition of 3, 5-dimethoxyaniline with aryl acid chlorides in the presence of triethyl amine provided intermediate A, which was treated with acyl chloride in the presence of tin chloride, followed by condensation reaction mediated by potassium *t*-butoxide under refluxing conditions (Scheme 1). The reaction sequence involves the amide bond formation via Schotten-Baumann reaction or aza-Michael addition followed by acylation/condensation reaction to provide the functionalized cores for series I-III in good yield. The intramolecular cyclization/condensation reaction of the aniline with an electrophile (intermediate B, Scheme 1), was mediated by modified thermal cyclization reaction conditions (diphenyl ether at 250 °C, in one-pot reaction sequence). Although, polyphosphoric acid can mediate such cyclization reactions, its corrosive nature and its high viscosity render work-up and the purification process challenging [11].

For the synthesis of the core quinolones for series II and III, substrate 3,5-dimethoxyaniline and 4-nitroaniline respectively were treated with dimethyl but-2-ynedioate in the presence of diphenyl ether to afford intermediate B, which was heated to form the desired product via intramolecular cyclization reaction in one-pot reaction sequence [11]. Consequently, the challenges posed by the purification of the products were circumvented by cooling the reaction vessel to RT, and rapidly adding hexane. The net effect of this binary solvent mixture enabled the precipitation of the desired product as a dark red powder, which was filtered and dried. Thus, our one-pot protocol afforded the quinolone product in nearly quantitative yield and avoided purification steps. To complete the synthesis of series III core, the corresponding nitro compound was reduced with Pd/C under a hydrogen atmosphere to yield the expected aniline product in excellent yield.

A preliminary survey of SAR was designed to assess potential liabilities related to the following concerns a) similar quinolone compounds display abroad range of biological properties, namely antimicrobial, antiviral, antimalarial activity, and mediated cyto- and geno-toxicity. Thus, our compounds were required to be evaluated in normal tissue (BJ cellular model) to avoid globally cytotoxicity, and b) comprehensive information regarding steric and electronic factors at the C2-C3 centers to provide guidance in generating a more appropriate quinolone system (Fig. 2). Compounds **7**–**16** were synthesized to evaluate the role of an aromatic versus the methyl ester at C-2, and the relevance of the introduction of the sulfonamide at *N*-1, followed by the evaluation of halogen groups at C3 center. Compounds **16**–**21** were synthesized to evaluate whether protecting groups influence biological activity.

To expand our evaluation of the molecular diversity that could be introduced at *N*-1, we proceeded to focus on sulfonamide synthesis (Fig. 3). Although numerous efforts have been made to modify quinolones [11], there are currently few reports concerning electrophilic substitutions at C-3 and direct *N*-modifications, which are governed by the C2-C3 substituents of the quinolone. Direct *N*-sulfonylation upon 2-aryl quinolone compound **7** was challenging using conventional conditions such as sulfonyl chloride in the presence of triethyl amine, as it provided *O*-sulfonylated compound **7b** as the sole product. After extensive experimentation, we were pleased to identify that copper mediated *N*-sulfonylation was highly efficient for this quinolone substrate **7** with great functional group tolerance, enabling the synthesis of quinolones with electron withdrawing or donating groups on the aryl sulfonamide moiety. Our findings extend the scope of utility for *N*-sulfonylation of quinolones without C-3 electron withdrawing directing groups, and also enable the direct *N*-sulfonylation on substituted anilines in

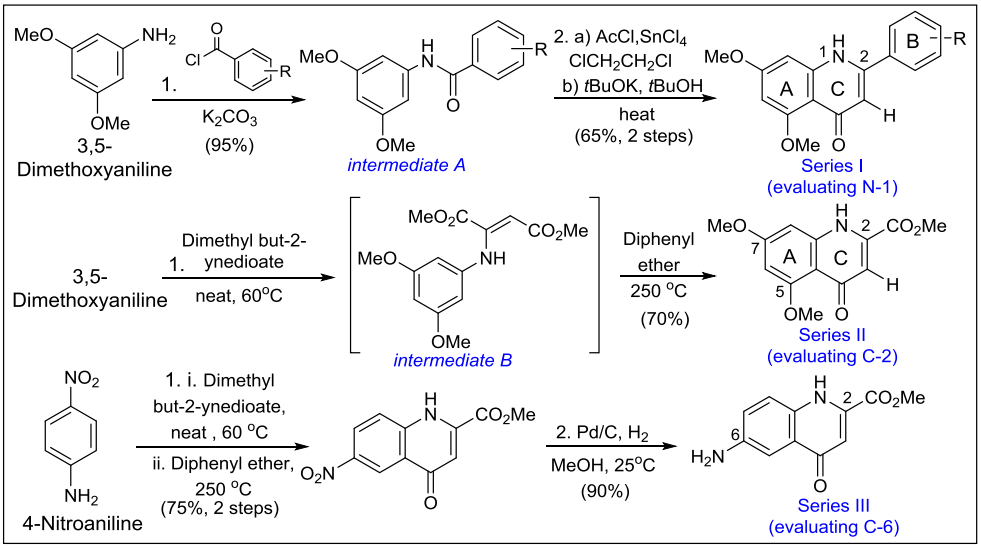

Scheme 1. General synthesis to 4-quinolone core series I-III.

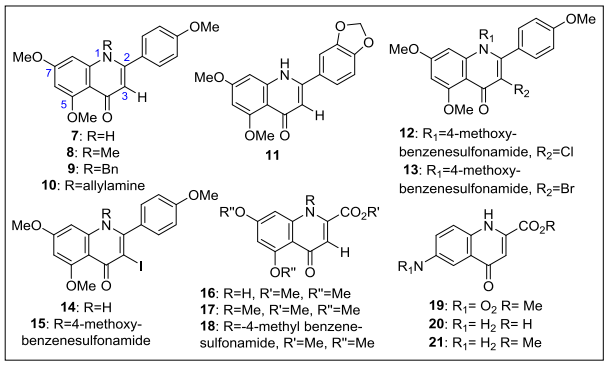

Fig. 2. Initial SAR evaluation: compounds **7**–**21**.

a quinolone motif. The optimal experimental conditions for the solvolysis of copper oxide required acetonitrile under refluxing conditions for 16 h. Thus, compound **7** was treated with the corresponding aromatic sulfonyl chloride reagents to provide **7a** as a single compound; **7b** was not detected by TLC or NMR analysis. The reaction proceeded in good yields for compounds **22**–**38**, which were purified as single products.

Amides are one of the most ubiquitous and important functional groups in natural and synthetic organic compounds so direct amidation of the ester **16** was a synthetic efficient option. Several conditions for the direct amidation were evaluated and found that the sodium bis(trimethylsilyl) amide (NaHMDS) amidation conditions were mild with high substrate generality for aromatic amines [12]. Thus, we employed this nucleophilic amidation upon compound **16** with a series of commercially available anilines. The substrates were treated with sodium bis(trimethylsilyl) amide (NaHMDS) in THF at RT. The base catalyzed amidation favored electronically rich anilines, with modest yields were obtained for electron deficient anilines. A plausible reaction mechanism is shown in Fig. 4. The reaction was sensitive to sterically demanding substrates or non-aromatic substrates, presumably not only due to the electronics, but also by the encumbered approach of the branched nucleophile. The reaction was allowed to stir for 24 h under an inert atmosphere to provide the desired products in good yields (**39**–**53**, Fig. 4). However, for compound **54**, this amidation conditions provided poor yields so the acid chloride of compound **16** was generated following the classic Schotten-Baumann reaction conditions [12]. Compound **16** was hydrolyzed and then treated with thionyl chloride to generate the corresponding acyl chloride, which was treated with the corresponding secondary amine substrate to provide the desired compound **54** in good yield.

Next, an exploration of solubility-enhancing substituents (such as the urea functionality) [13] at the C6 position of the aromatic ring was an appropriate step to enable cellular permeability, and evaluate the influence of the substituents of this scaffold. In addition, the role of the methoxy groups could be compared with other heteroatoms. Compound **21** was treated with the corresponding electrophiles in DMF at RT for 12 h, affording the desired quinolone-urea compound in good yield (Fig. 5).

2.1. Inhibition of proliferation by new compounds

A heat map of the anti-proliferative activity in ALL models (KOPN8, SEM, SUP-B15 and UoCB-1) in comparison to normal tissue models (BJ, THLE-2) using established CelTiter-Glo® cell viability protocol [13] is shown in Table 1. While vitexin has been disclosed to have activity against U937 lymphoma cellular model [7], we did not observe cytotoxicity against Raji (Burkitt lymphoma cellular model at the tested concentrations up to 100 μM using CelTiter-Glo®). Several of these analogues displayed promising biological activity, while compounds **19**–**25**, **30**–**42**, **46**–**53**, **64**–**66**, and **73** showed no cytotoxicity at the tested concentrations (see SI).

While several leukemia cellular models were utilized for our viability assays, we focused our attention on compounds with cytotoxicity against a particular subset of acute lymphoblastic leukemia: KOPN-8, SEM, and SUP-B15 models, all of which carry specific genomic lesions. KOPN-8 carries the MLL-ENL fusion gene, SEM is a carrier of t(4, 11) fusion gene (MLL-AF4), and SUP-B15 was established from a pediatric ALL relapsed patient (with the m-BCR ALL variant of the BCR-ABL1 fusion gene) [14]. The gene for the histone methyltransferase MLL participates in chromosomal translocations that eventually create MLL-fusion proteins associated with very aggressive forms of childhood acute leukemia. The presence of some MLL rearrangements is an independent dismal prognostic factor and patients are usually treated according to high-risk protocols [3,4]. Therefore, the identification of

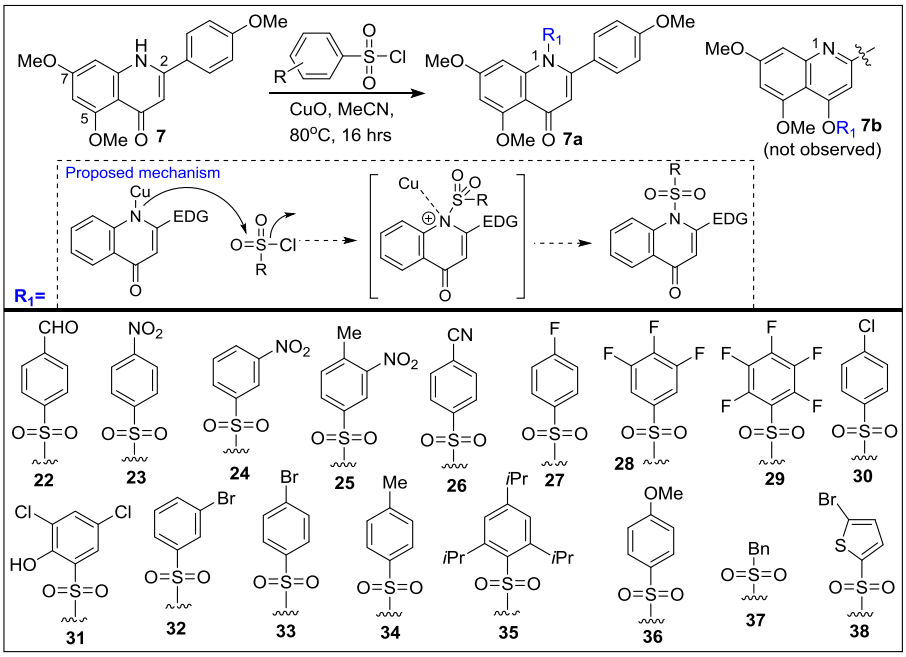

Fig. 3. Synthesis of *N*-1 substituted compounds **22**–**38**.

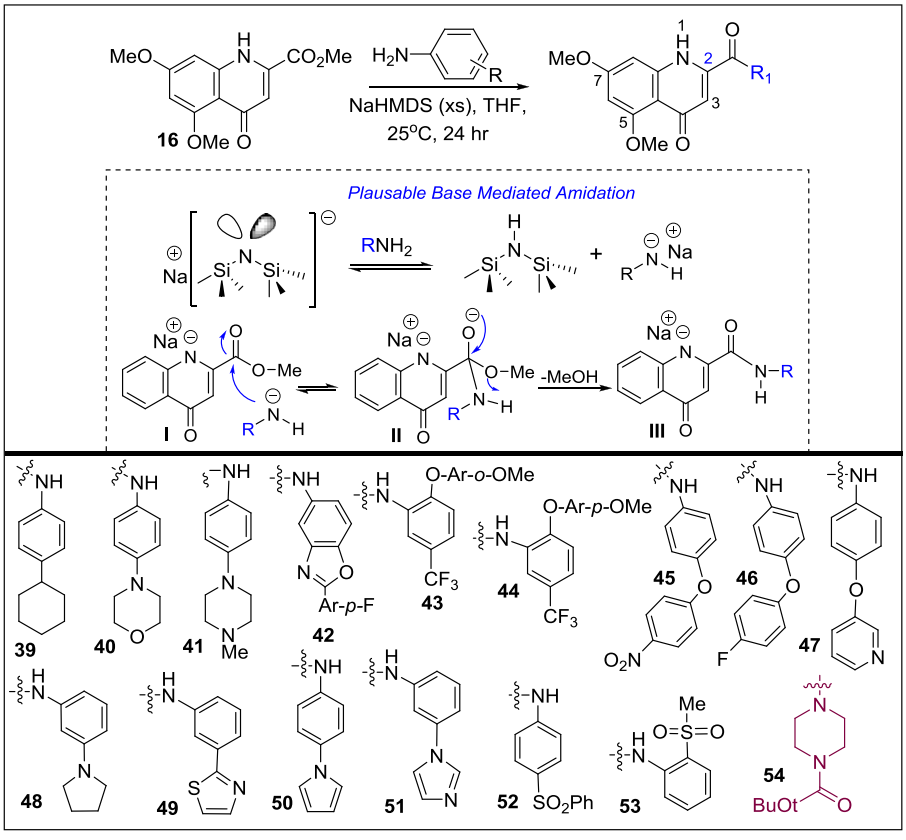

Fig. 4. Synthesis of C2 substituted quinolone compounds **39**–**54**.

compounds against models with MLL gene fusions is necessary for the discovery of new therapies.

While quinolones have been reported to exert various biological activities, but mainly antibiotic properties [15], we questioned the possibility that they were inhibiting CDK9. The selectivity and potency of flavopiridol, **4** towards CDK9 has been attributed to the 4-keto, 6-phenyl ether interacting at the CDK9 hinge as a hydrogen donor and acceptor between amino acid Asp104 and Cys106. The

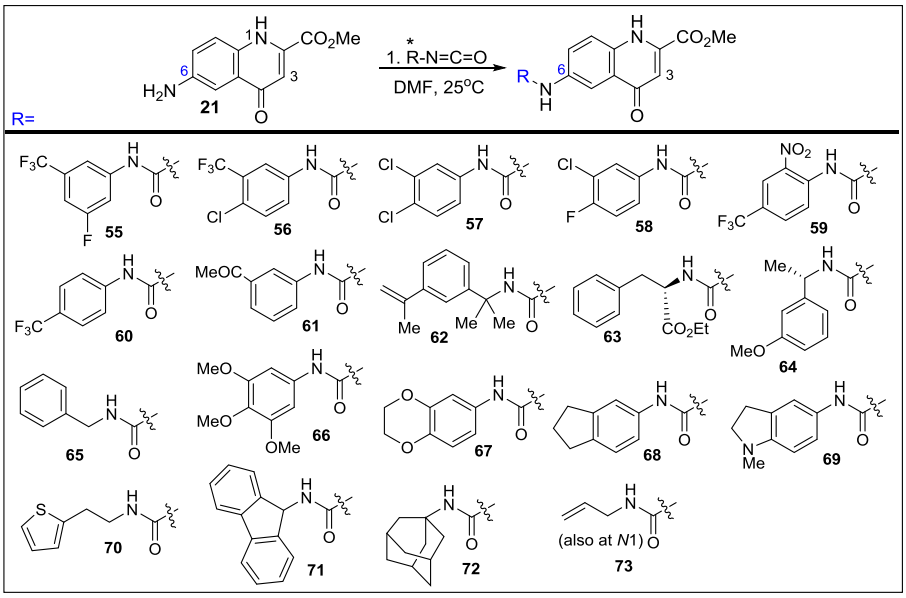

Fig. 5. Synthesis of C6 substituted urea compounds **55**–**73**.

Table 1
Representative heat map of selected compounds.

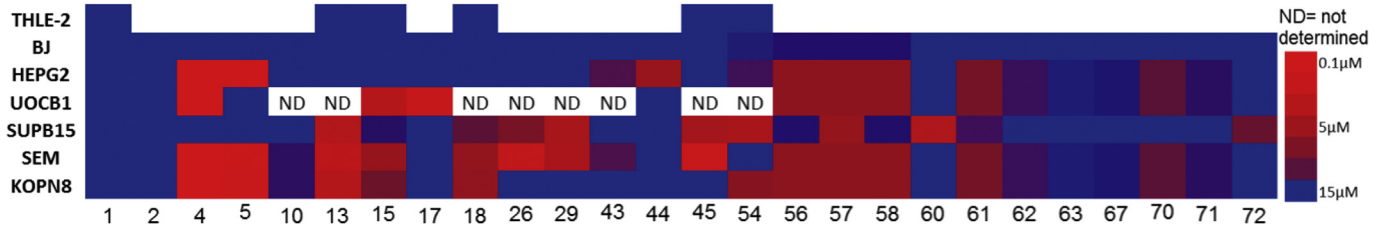

remaining of the molecule can engage in π-stacking from the B ring and hydrophobic interactions [13]. With a dihedral angle of 122°, the chromen C ring is slightly different from our quinolone core with an angle of 118°, which is forced to maintain the pyramidal structure of the amine (Fig. 10A). However, the α-halogens influence the binding affinity of the enone to accept protons. In fact, the dehalogenated compounds had weaker activity. However, the sulfonamides such as compound **18**, are active in the low micromolar range (5–6 μM) against KOPN-8 and SEM, and it showed less activity (10 μM) against SUP-B15. The urea compounds **54**, **56**–**58** also showed promising activity against ALL cellular models and further mechanistic studies will be conducted to evaluate which amino acids are interacting with the carbamide group. Current SAR among these compounds shows an activity trend based on the placement and nature of the substituents of the aromatic ring at the NH at C6 against KOPN-8 and SEM. A few of these compounds showed selectivity for SUP-B15, such as compounds **29**, **60**, and **72**. Compound **60** showed more promising activity ($EC_{50} = 3.2$ μM) than compound **72** ($EC_{50} = 9.1$ μM) against SUP-B15. An interesting observation for these latter compounds is their lack of SAR. Thus, further biochemical assays combined with structural biological studies will be pursued to answer this question. For instance, compound **55** having meta-fluoride substituents showed no activity against SUP-B15 at the tested concentrations (≤30 μM) yet the para-fluoride substituent **60**, showed potency, selectivity towards this cell line and therapeutic window in BJ cells. Addition of moderately small groups, or bulky groups (9-methyl-9H-fluorene) to the urea, such as alkyl phenyl, heterocycles (furan, indole), introduction of ethers (trimethoxy, dioxane) did not substantially improve their biological profile ($EC_{50} > 15$ μM) against these cellular models.

The results indicate the methoxy groups at the A ring of the molecule might not play a significant role in the biological activity observed. It is also possible that our compounds (series I-III) might not act on the same target as the SAR among them is not clearly defined. Gratifyingly, our compound series provided compounds (**13**, **15**, **18** from series I, **54** from series II and **56**–**58** from series III) with improved biological activity than vitexin. Further mechanistic studies and fine tuning to improve solubility on these compounds will be conducted.

2.2. Compound 15 induces G0/G1 cell cycle arrest

Fluorochrome-labeled Annexin V and DNA content [16] with PI were studied in treatment with compounds **15**, **54**, and **56** for a 24 h period in KOPN-8 and SUP-B15 (see SI) to confirm apoptosis. Representative images for negative control (DMSO), positive control (2.0 μM staurosporine) and compound **4** (5.0 μM) for 24 h treatment are shown. Data presented on compounds **15**, **54**, and **56** (D-F, Fig. 6) clearly captured the increase of late apoptotic state (Q2) upon compound treatment with a modest amount observed for compound **54**.

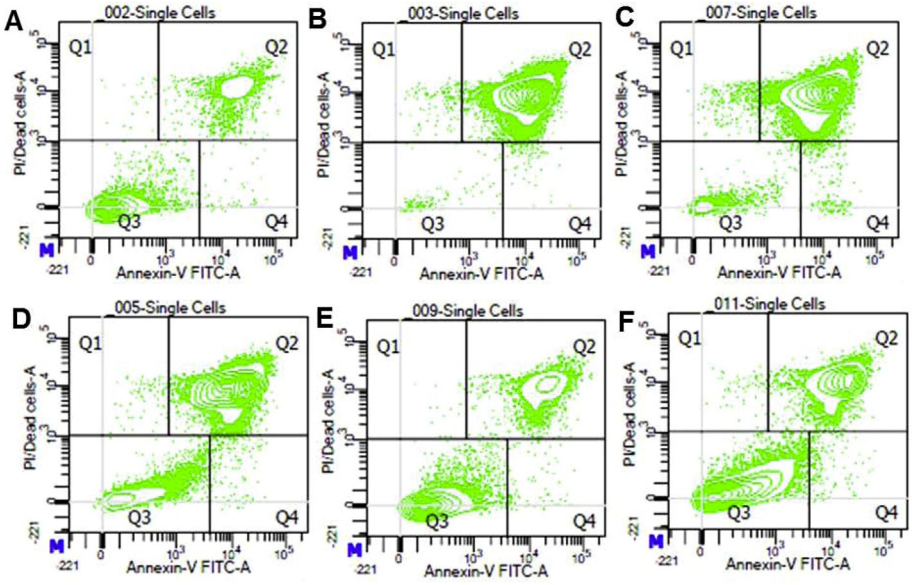

Fig. 6. Representative of FITC Annexin V apoptosis, and Propidium Iodide (PI) staining after 24 h in KOPN-8 cellular model. **A.** vehicle control (DMSO). **B.** positive control (2 μM staurosporine) **C.** Compound **4** (5 μM). **D.** Compound **15** (10 μM). **E.** Compound **54** (10 μM). **F.** Compound **56** (10 μM).

Next, DNA content of KOPN-8 cells was measured to interrogate cell cycle effects compared with flavopiridol, **4**. Proliferating cells progress through various phases of the cell cycle (G0, G1, S, G2, and M phase) and CDKs are important regulators of cell cycle [17]. No serum starvation or chemical-induced synchronization methods were used for ALL cellular models to avoid potential secondary effects due to such manipulation [18], however, synchronization was performed in a validated cellular model (MDA-MB231 cell lines, see SI for data) to capture any differences. Graphical quantitation of the respective cell cycle phases for compound **15**, **54**, and **56** at 10–20 μM versus controls (DMSO negative control, staurosporine and compound **4** as positive controls) for 24 h is shown in Fig. 7. Cell cycle arrest occurred in the G0/G1 phase at 10 μM concentration for compounds **15** and **56** as compared to controls. At this concentration, ~15–20% of cells accumulated at G0/G1 phase, indicating inhibition of the pre-replicative phase, and initiation of apoptosis was also observed by Annexin V. The DMSO control indicates that the cells were primarily at the S phase at the time of the experiment and only a small number (10%) were entering the G2/M. Compound **15** distributed the cells in a similar manner to the cytotoxic staurosporine, but showed a slightly increase at the G2/M phase, a phenomenon also observed for compound **5**. Data are shown from at least three independent experiments. Statistical analysis of data was performed using Graph Pad Prism 5 and Microsoft Excel software. The differences between the groups were analyzed by *t*-test. Standard error bars represented the standard deviation of the mean (±SD).

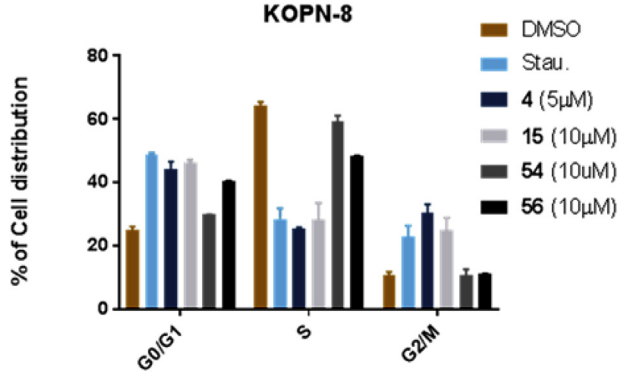

Fig. 7. KOPN-8 cell cycle distribution upon compound treatment. Compound **15** effects on cell cycle were similar to compound **4**, while compounds **54** and **56** had less effects on the cycle compared to controls.

2.3. Cell death validation and potential biological targets

To further examine the effects of compound **15** in comparison to clinical compounds **4**, and **5**, and to gain understanding on how compound **15** causes cell death, additional cellular experiments were conducted (Figs. 8 and 9). Because quinolone compounds have the potential to react with glutathione, the precursor *N*-acetyl cysteine (NAcCys) was also added to a set of cells to investigate whether 1, 4-Michael addition reactions would prevent cell death.

As shown in Fig. 8, compound **15** (10–100 μM final concentration) caused cell death in a dose dependent manner as shown by PARP-cleavage after 3 and 24 h. In the NAcCys treated cells, little to no PARP cleavage was observed at 3 h for the higher concentrations, presumably due to its anti-oxidant effect. However, it was detected at the higher dose at 24 h.

Similarly compound **5** induced PARP cleavage after 3 h, but not at 24 h. The addition of NAcCys in combination to compound **5** had similar effects as compound **15**. Compound **4** treated cells showed consistent levels of PARP cleavage over time with or without anti-oxidant. Then, the expression levels of the short-lived anti-apoptotic factor Mcl-1 were investigated as blocking CDK9 removes its ability to inhibit apoptosis [19]. Both compounds **4** and **5** suppressed expression of Mcl-1, and compound **15** showed a similar pattern in a dose dependent manner.

To interrogate the signaling of cyclin dependent kinases, we turned our attention to the positive transcription elongation factor b (P-TEFb, which consists of CDK9 and cyclin T1 or T2) complex. P-TEFb is recruited to RNA polymerase II transcription initiation complexes, where P-TEFb phosphorylates the transcription elongation factors DRB sensitivity inducing factor (DSIF), the negative elongation factor (NELF) and the C-terminal domain (CTD) of the

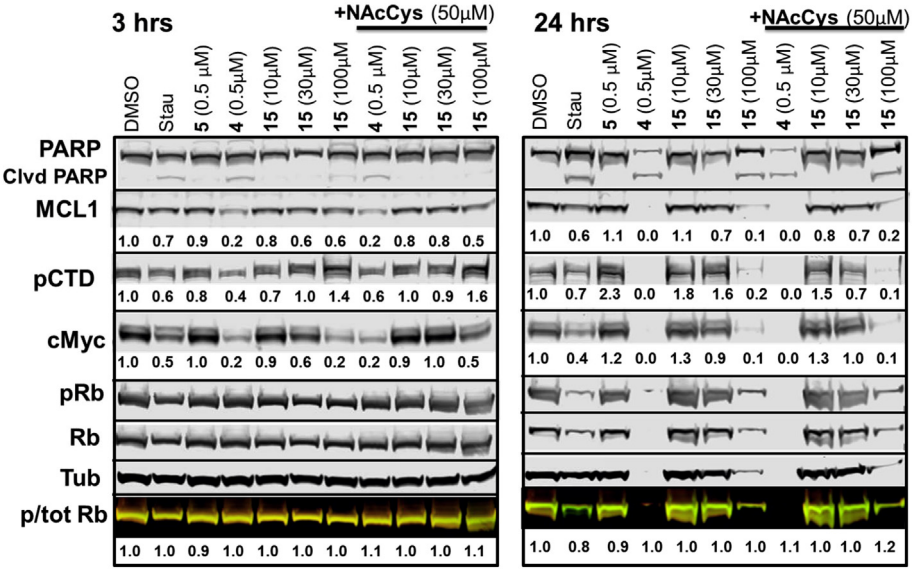

Fig. 8. Western analysis of KOPN-8 cellular line treated with compound **15** and control compound **4**–**5** for 3, and 24 h respectively.

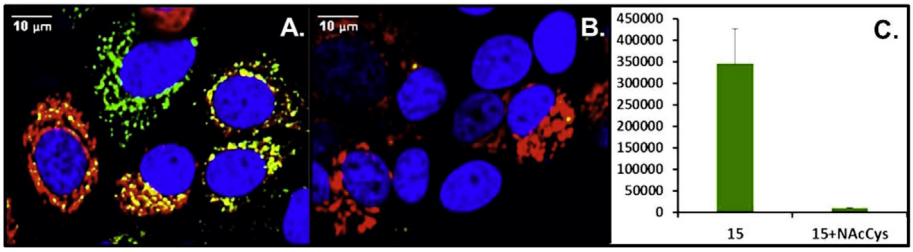

Fig. 9. Reactive oxidative species (ROS) studies of compound **15**. **A.** MCF7-Ruby red labeled (Cox8A-mitochondria) cells treated with 50 μM **15** alone. **B.** 50 μM **15** along with 50 μM NAcCys for 1 h, followed by staining with CellROX® green reagent and nuclear stain Hoechst 33342 (blue). **C.** ROS relative quantification. (For interpretation of the references to colour in this figure legend, the reader is referred to the Web version of this article.)

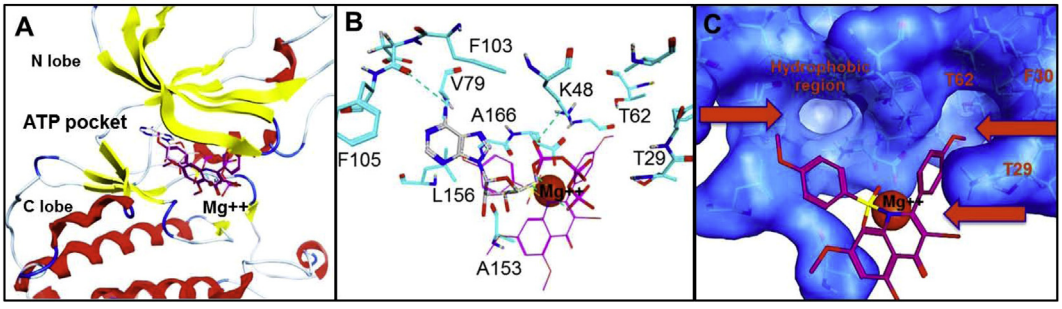

Fig. 10. Predicted binding mode of compound **15** to CDK9 using MOE program. **A.** Protein surface and compound **15**. **B.** Top close view of interactions between compound **15** (magenta) and the hinge region of the ATP binding site, (ATP gray) and interacting amino acids (cyan). **C.** Surface representation of ATP pocket of CDK9, with compound **15** bound (magenta). Red arrows indicate regions for chemical space exploration. (For interpretation of the references to colour in this figure legend, the reader is referred to the Web version of this article.)

largest subunit of RNA polymerase II, thereby enabling transcription complexes to transition into the productive elongation phase [20–22]. Work by Chao has demonstrated inhibition of RNAPII elongation by compound **4**, resulting in abortive transcription of most protein coding genes [22]. Both compounds **4** and **5** caused a decrease in the levels of phosphorylated Ser-2 of the CTD after 3 h with recovery recorded for compound **5**, but not for compound **4** after 24 h. Compound **15** showed a decrease in Ser-2 phosphorylation CTD levels in a dose dependent manner at 24 h. The cMyc expression decreased in dose dependent manner for compound **15**, with no substantial change for compound **4**.

Finally, we evaluated the phosphorylation levels of the Retinoblastoma tumor suppressor protein (Rb) critical to multiple cellular activities related to cell cycle. Rb is rarely mutated in human cancers, instead regulatory pathways that alter Rb activity by phosphorylation at CDK sites are altered [22]. Recent studies indicate that CDK4/6 activates Rb for binding cellular targets during early G1 phase, which results in Rb mono-phosphorylation to drive

quiescent G0 cells into a more metabolically active, but early G1 phase arrested phenotype [16]. The constitutively mono-phosphorylated Rb neoplastic cell avoids cell cycle exit and differentiation, so we evaluated changes in Rb phosphorylation in our compound treated KOPN-8 cells. Little to no change was recorded after 3 h, while less expression of total Rb and pRb was observed in a dose dependent manner for compound **15** after 24 h treatment. After 72 h, extensive cell death was recorded, limiting the detection of these proteins (data not shown). At the 24 h time point, compound **15** showed reduction in pRb in a dose dependent manner similarly to the observed effects of compound **4**. The combined findings suggest that CDK9 is a potential target (s) of the described compounds. However, further mechanistic studies are warranted to confirm this speculated biological target.

Eleven Nineteen Leukemia (ENL) and AF4 proteins, common associating partners of MLL in childhood acute leukemia are known to bind and utilize P-TEFb for their transformation properties [21], thus highlighting why compound such as **15** have better potency in subtypes of ALL cellular models. This suggests that therapies targeting P-TEFb activity in leukemia might be a direction to pursue for refining precision therapeutics.

2.4. Compound 15 induces oxidative stress in live cellular models

A high level of oxidative phosphorylation represents a liability to tumor cells due to the role of mitochondria in apoptosis, and generation of ROS is carefully regulated [23]. Live cell CellROX® experiments were conducted to evaluate if our lead compounds trigger intrinsic apoptotic pathways by inducing reactive oxygen species (ROS) since reduced Mcl-1 expression and CDK inhibition had been recorded. CellROX® green reagent is a cell-permeable dye with weak fluorescence while in a reduced state, and exhibits bright green photostable fluorescence upon oxidation by ROS (with absorption/emission maxima of 485/520 nm) [24]. A representative experiment is shown in Fig. 9. The mRuby-Cox8A [25] labeled MCF-7 cellular model was treated with compound **15** (Fig. 9A) or treated with **15** along with ROS quencher, NAcCys for 1 h, followed by CellROX® green reagent addition, and relative quantification (Fig. 9B and C). Compound **15** clearly increased total ROS, particularly mitochondria-derived ROS (orange, Fig. 9A). The cells exposed to NAcCys were distinctly protected against ROS, as it presumably increases glutathione levels, which bind to either the toxic breakdown products generated from **15**, or directly to **15**. To further assess the latter possibility, LC-MS analysis of incubation of compound **15** in DMSO with NAcCys or with glutathione for 1 h at 37 °C did not detect any potential 1,2 or 1,4 Michael addition products.

2.5. Molecular docking studies

Protein kinase structural studies have shown that the adenine moiety of adenosine triphosphate (ATP) docks into a hydrophobic cleft between the two lobes of the kinase domain of CDK4/6 and 9, interacting with the kinase hinge region through hydrogen bonding. Several inhibitors of these CDKs are known to bind at this conserved nucleotide binding site. For instance, compound **4** establishes ATP-like hydrogen bond interactions with CDK2, CDK4/6, and CDK9 in complex with cyclin T domain binding cleft by computational docking studies coupled with co-crystallographic data [26].

To elucidate whether our compounds were interacting with the CDKs in a similar binding mode to compound **4** and **5**, molecular docking studies of these compounds with CDK4/6 and CDK9 were performed. Homology models of CDK4 and CDK9 were built with MOE from the ATP bound conformation of CDK2 (PDB code: 1qmz) [26]. In addition, a magnesium ion was included in the same location as observed in the 1qmz model. A local minimization of nearby residues was performed to facilitate the octahedral coordination geometry between protein residues and magnesium ion. The CDK2 with a derivative of flavopiridol (L868276) complex shows that the inhibitor binds at the ATP binding site. The protein is folded into the typical bilobal structure with the N-terminal domain consisting predominantly of β-sheet structures, and the C-terminal domain consisting mainly of alpha helices [26].

We predicted the interactions of compound **15** with the CDKs could be driven by hydrophobic and van der Waals interactions with the amino residues that form the pocket for the adenine base in the ATP-CDK2 protein complex. To test such hypothesis, compound **15** and compound **13** were docked into the cleft of CDK4 and CDK6 using the Glide docking tool in Maestro [27]. However, both CDK4 and CDK9 provided low docking scores indicating additional effects from solvent or protein rearrangement might be important contributors to the binding modes, which were not captured by our solvent free flexible ligand docking studies.

Compounds **13** and **15** showed similar binding mode for CDK9, which was lacking in the CDK4 studies, supporting our experimental data. The docked compound **15** (magenta) in the binding cleft of CDK9 overlaid on the ATP from our working template 1qmz [26], is depicted in Fig. 10A. A close-up image (Fig. 10B) showcases the docked ligand interactions with the hydrophobic residues L156, V79, A166, A153 and the aliphatic chain of LYS48 in the CDK9 homology model. A hydrogen-π interaction between Ala153 and the quinolone motif was observed while no significant overlap between the ATP adenosine ring and compound **15** were observed.

Furthermore, the sulfonyl group of this compound interacts favorably with the magnesium ion. Additional molecular interactions could be exploited at the indicated sites (red arrows, Fig. 10C) to increase binding affinity. Our combined molecular studies highlight the restricted ATP pocket as a potential region to explore in order to improve selectivity and potency for our lead compounds (**13**/**15**) as they bind differently to CDK9 from CDK4 in the docked models. The differences in pose and docking scores indicate the divergence in how these compounds interact with the CDK9 cleft region, emphasizing opportunities for selectively targeting these isoforms. Our studies also suggest the 2-methoxy phenyl ring could grow into the pocket made by Thr62, Phe30 and Thr29 to improve its binding affinity (Fig. 10C). Furthermore, the study shows that coordinating groups on the sulfonamide could improve potency through chelation with the magnesium ion. The methoxy group of the aromatic sulfonamide fits in the hydrophobic pocket lined by F103 and V79, which can accommodate larger alkyl/Ar groups to increase favorable interactions in this region. Hydrogen bond acceptors or donors may also provide interactions with the backbone of F105 and D104. Molecular dynamic studies with explicit solvent are warranted to better understand their binding mode and develop more potent compounds.

2.6. Conclusion

In summary, a new series of 4-quinolone compounds inspired by the natural product vitexin was developed using a simplified and scalable synthetic protocol using readily available reagents. Compounds **12**–**15** represent a novel anticancer sulfonamide scaffold class with similar mechanism of action to CDK inhibitors and share similar chemical properties to flavopiridol. As depicted in Table 1, the halogenated 4-quinolon-*N*-sulphonamides displayed promising biological activity and selectivity towards specific ALL cellular models. Our cellular evaluation indicate halogenated sulfonamides (**12**–**15**) show anti-proliferative effects preferentially against MLL-ALL cellular models, while the urea derivatives (**55**–**73**) displayed anti-proliferative effects across most ALL cellular models tested

with therapeutic window in non-tumor cellular mode (BJ) of at least 10 fold.

This study is significant as: (a) we have developed a protocol to access 4-quinolon-core scaffolds in one-pot reaction, followed by a direct *N*-sulfonylation reaction of these quinolones which enables the synthesis of a diverse group of compounds (b) while chromanflavones are well documented from a biological perspective, our 4-quinolon-core offers a new scaffold that will serve as a chemical probes to better understand high risk ALL cellular subtypes and better understand the biological mechanisms that drive them, and (c) our study illustrates the importance of natural products as valuable tools for drug discovery as they have provide the foundation for a targeted-driven medicinal chemistry program against high risk ALL subtypes. The combined results warrant future studies to elucidate the exact mechanism of action of these novel 4-quinolones as selective agents against high risk ALL.

Conflicts of interest

The authors declare that they have no competing interests.

Acknowledgments

This study was supported by the American Lebanese Syrian Associated Charities (ALSAC). The authors thank the Analytical Technologies Center Core Facility for analytical support, the Flow and Cell Cycle Facility and the Cell and Tissue Imaging Center Microscopy for technical assistance at St. Jude Children's Research Hospital.

Appendix A. Supplementary data

Supplementary data related to this article can be found at https://doi.org/10.1016/j.ejmech.2018.01.004.

References

[1] a) G. Tallen, R. Ratei, G. Mann, et al., Long-term outcome in children with relapsed acute lymphoblastic leukemia after time-point and site-of-relapse stratification and intensified short-course multidrug chemotherapy: results of trial ALL-REZ BFM 90, J. Clin. Oncol. 28 (2010) 2339–2347;
b) Cancer Trends Progress Report– 2009/2010 Update, National Cancer Institute, NIH, DHHS, Bethesda, MD, April 2013. http://progressreport.cancer.gov;
c) The Leukemia & Lymphoma Society, (Accessed 10 February 2017). http://www.lls.org/.

[2] a) C.H. Pui, W.E. Evans, Treatment of acute lymphoblastic leukemia, N. Engl. J. Med. 354 (2006) 166–178;
b) C.G. Mullighan, et al., Genomic analysis of the clonal origins of relapsed acute lymphoblastic leukemia, Science 322 (2008) 1377–1380.

[3] a) C. Meyer, J. Hofmann, T. Burmeister, et al., The MLL recombinome of acute leukemias in 2013, Leukemia 27 (2013) 2165–2176;
b) A.K. Anderson, J. Ma, J. Wang, et al., The landscape of somatic mutations in infant MLL-rearranged acute lymphoblastic leukemias, Nat. Genet. 47 (2015) 330–337;
c) R. Marschalek, Mechanisms of leukemogenesis by MLL fusion proteins, Br. J. Haematol. 152 (2010) 141–154;
d) A.K. Anderson, J. Ma, J. Wang, et al., The landscape of somatic mutations in infant MLL-rearranged acute lymphoblastic leukemias, Nat. Genet. 47 (2015) 330–337.

[4] a) E. Etienne De Braekeleer, et al., Identification of *MLL* partner genes in 27 patients with acute leukemia from a single cytogenetic laboratory, Mol. Oncol. 5 (2011) 555–563;
b) M. Dordelmann, A. Reiter, et al., Prednisone response is the strongest predictor of treatment outcome in infant acute lymphoblastic leukemia, Blood 94 (1999) 1209–1217.

[5] a) M. He, J.W. Min, W.L. Kong, X.H. He, J.X. Li, B.W. Peng, A review on the pharmacological effects of vitexin and isovitexin, Fitoterapia 115 (2016) 74–85;
b) J.H. Kim, B.C. Lee, J.H. Kim, G.S. Sim, D.H. Lee, K.E. Lee, Y.P. Yun, H.B. Pyo, The isolation and antioxidative effects of vitexin from Acer palmatum, Arch Pharm Res. 28 (2005) 195–202;
c) M. Bhardwaj, S. Paul, R. Jakhar, S.C. Kang, Potential role of vitexin in alleviating heat stress-induced cytotoxicity: regulatory effect of Hsp90 on ER stress-mediated autophagy, Life Sci. 142 (2015) 36–48.

[6] a) H. Takahashi, M.C. Chen, H. Pham, E. Angst, J.C. King, J. Park, E.Y. Brovman, H. Ishiguro, D.M. Harris, H.A. Reber, O.J. Hines, A.S. Gukovskaya, V.L. Go, G. Eibl, Baicalein, a component of Scutellaria baicalensis, induces apoptosis by Mcl-1 down-regulation in human pancreatic cancer cells, Biochim. Biophys. Acta 13 (2011) 1465–1474;
b) G. Wei, B. Yu, Isoflavone glycosides: synthesis and evaluation as α-glucosidase inhibitors, Eur. J. Org. Chem. (2008) 3156–3163;
c) G. Lewin, A. Maciuk, A. Moncomble, J.-P. Cornard, Enhancement of the water solubility of flavone glycosides by disruption of molecular planarity of the aglycone moiety, J. Nat. Prod. 76 (2013) 8–12.

[7] a) J. Zhou, H. Hu, J. Long, F. Wan, L. Li, S. Zhang, Y.E. Shi, Y. Chen, Vitexin 6, a novel lignan, induces autophagy and apoptosis by activating the Jun N-terminal kinase pathway, Anti Canc. Drugs 24 (2013) 928–936;
b) C.Y. Lee, Y.S. Chien, T.H. Chiu, W.W. Huang, C.C. Lu, J.H. Chiang, J.S. Yang, Apoptosis triggered by vitexin in U937 human leukemia cells via a mitochondrial signaling pathway, Oncol. Rep. 28 (2012) 1883–1888;
c) Y. Zhou, Y.E. Liu, J. Cao, G. Zeng, C. Shen, Y. Li, M. Zhou, Y. Chen, W. Pu, L. Potters, Y.E. Shi, Vitexins, nature-derived lignan compounds, induce apoptosis and suppress tumor growth, Clin. Canc. Res. 15 (2009) 5161–5169;
d) J. Lee, T. Park, S. Jeong, K.-H. Kim, C. Hong, Hydroxychromones as cyclin-dependent kinase inhibitors: synthesis and biological evaluation, Bioorg. Med. Chem. Lett 17 (2007) 1284–1287.

[8] J.K. Brunelle, et al., Loss of Mcl-1 protein and inhibition of electron transport chain together induce anoxic cell death, Mol. Cell. Biol. 27 (2007) 1222–1235.

[9] C. LaCerte, V. Ivaturi, J. Gobburu, J.M. Greer, L.A. Doyle, J.J. Wright, J.E. Karp, M.A. Rudek, Exposure-response analysis of alvocidib (Flavopiridol) treatment by bolus or hybrid administration in newly diagnosed or relapsed/refractory acute leukemia patients, Clin. Canc. Res. (2017). CCR-16–2629.

[10] a) M. Russo, G.L. Russo, M. Daglia, P.D. Kasi, S. Ravi, S.F. Nabavi, S.M. Nabavi, Understanding genistein in cancer: the "good" and the "bad" effects: a review, Food Chem. 196 (2016) 589–600;
b) S.-J. Li, S.-L. Sun, J. Gao, F.-B. Sun, Wogonin induces Beclin-1/PI3K and reactive oxygen species-mediated autophagy in human pancreatic cancer cells, Oncol. Lett. 12 (2016) 5059–5067;
c) A. Uifălean, S. Schneider, C. Ionescu, M. Lalk, C.A. Iuga, Soy isoflavones and breast cancer cell lines: molecular mechanisms and future perspectives, Molecules 21 (2015), E13;
d) G. Polier, J. Ding, B.V. Konkimalla, D. Eick, N. Ribeiro, R. Köhler, M. Giaisi, T. Efferth, L. Desaubry, P.H. Krammer, M. Li-Weber, Wogonin and related natural flavones are inhibitors of CDK9 that induce apoptosis in cancer cells by transcriptional suppression of Mcl-1, Cell Death Dis. 21 (2011), 2:e182.

[11] a) D.H.A. Rocha, D.C.G.A. Pinto, A.M.S. Silva, Synthesis and cyclisation studies of (E)-2-aryl-1-methyl-3-styrylquinolin-4(1H)-ones, Tetrahedron 71 (2015) 7717–7721;
b) X. Gu, G.I. Georg, Regioselective C5-alkylation and C5-methylcarbamate formation of 2,3-dihydro-4-pyridones and C3- alkylation and C3-methylcarbamate formation of 4-(pyrrolidin-1-yl)furan-2(5*H*)-one, Tetrahedron Lett. 56 (2015) 5874–5877;
c) R. Cincinelli, L. Musso, G. Beretta, S. Dallavalle, 4-Quinolone fused heterocyclic ring systems byintramolecular reactions of 4-quinolone-2-carboxamides, Tetrahedron 70 (2014) 9797–9804;
d) J.-G. Kim, D.O. Jang, Mild and efficient indium metal catalyzed synthesis of sulfonamides and sulfonic esters, Synlett 16 (2007) 2501–2504;
e) M.E. Rodriguez, D.A. Mareska, J.J. Hans, D.M. Harvey, R.D. Groneberg, M. O'sullivan (2010). Piperidine-containing compounds and use thereof, Google Patents WO 2010080864 A1. f) G.A. Meshram, D. Patil, Vishvanath, A simple and efficient method for sulfonylation of amines, alcohols and phenols with cupric oxide under mild conditions, Tetrahedron Lett. 50 (2009) 1117–1121;
g) D. Zewge, C.-Y. Chen, C. Deer, P.G. Dormer, D.L. Hughes, A mild and efficient synthesis of 4-quinolones and quinolone heterocycles, J. Org. Chem. 72 (2007) 4276–4279;
h) C.P. Jones, K.W. Anderson, S.L. Buchwald, Sequential Cu-catalyzed amidation-base-mediated camps cyclization: a two-step synthesis of 2-Aryl-4-quinolones from o-halophenones, J. Org. Chem. 72 (2007) 7968–7973;
i) I. Borza, S. Kolok, K. Galgóczy, A. Gere, C. Horváth, S. Farkas, I. Greiner, G. Domány, Kynurenic acid amides as novel NR2B selective NMDA receptor antagonists, Bioorg. Med. Chem. Lett. 17 (2007) 406–409;
j) D. Ding, X. Li, X. Wang, Y. Du, J. Shen, Microwave-assisted rapid and straightforward synthesis of 2-aryl-4-quinolones from acylated 2′-aminoacetophenones, Tetrahedron Lett. 47 (2006) 6997–6999.

[12] a) D.A. Nugiel, J.R. Krumrine, D.C. Hill, J.R. Damewood Jr., P.R. Bernstein, C.D. Sobotka-Briner, J.W. Liu, A. Zacco, M.E. Pierson, *De novo* design of a picomolar nonbasic 5-HT1B receptor antagonist, J. Med. Chem. 53 (2010) 1876–1880;
b) R.S. Varma, K.P. Naicker, Solvent-free synthesis of amides from non-enolizable esters and amines using microwave irradiation, Tetrahedron Lett. 40 (1999) 6177;
c) L. Perreux, A. André Loupy, M. Delmotte, Microwave effects in solvent-free esters aminolysis, Tetrahedron 59 (2003) 2185–2189.

[13] a) I.H. Kim, H.J. Tsai, K. Nishi, T. Kasagami, C. Morisseau, B.D. Hammock, 1,3-disubstituted ureas functionalized with ether groups are potent inhibitors of the soluble epoxide hydrolase with improved pharmacokinetic properties, J. Med. Chem. 50 (2007) 5217–5226;

b) K. Mitachi, Y.G. Salinas, M. Connelly, N. Jensen, T. Ling, F. Rivas, Synthesis and structure-activity relationship of disubstituted benzamides as a novel class of antimalarial agents, Bioorg. Med. Chem. Lett. 22 (2012) 4536–4539;
c) J.H. Zhang, T.D. Chung, K.R. Oldenburg, A simple statistical parameter for use in evaluation and validation of high throughput screening assays, J. Biomol. Screen 4 (1999) 67–73.

[14] H.G. Dexler, Guide to Leukemia and Lymphoma Cell Lines, second ed., 2010. German Collection of microorganisms and cell cultures Braunschweig, Germany.

[15] a) M.L. Bolognesi, R. Banzi, M. Bartolini, A. Cavalli, A. Tarozzi, V. Andrisano, A. Minarini, M. Rosini, V. Tumiatti, C. Bergamini, R. Fato, G. Lenaz, P. Hrelia, A. Cattaneo, M. Recanatini, C. Melchiorre, Novel class of quinone-bearing polyamines as multi-target-directed ligands to combat Alzheimer's disease, J. Med. Chem. 50 (2007) 4882;
b) Y.X. Yu, J.M. Hill, G. Yu, Y. Yang, A.F. Kluge, D. Keith, J. Finn, P. Gallant, J. Silverman, A. Lim, A series of quinoline analogues as potent inhibitors of C. albicans prolyl tRNA synthetase, Bioorg. Med. Chem. Lett. 11 (2001) 541.

[16] a) M.B. Kastan, J. Bartek, Cell-cycle checkpoints and cancer, Nature 432 (2004) 316–323;
b) C. Riccardi, I. Nicoletti, Analysis of apoptosis by propidium iodide staining and flow cytometry, Nat. Protoc. 1 (2006) 1458–1461;
c) L. Galluzzi, et al., Cell Death Differ. 19 (2012) 107–120.

[17] a) C.J. Sherr, F. McCormick, The RB and p53 pathways in cancer, Canc. Cell 2 (2002) 103–112;
b) Y.J. Choi, L. Anders, Signaling through cyclin D-dependent kinases, Oncogene 33 (2014) 1890–1903.

[18] U. Kim, C.W. Shu, K.Y. Dane, P.S. Daugherty, J.Y. Wang, H.T. Soh, Selection of mammalian cells based on their cell-cycle phase using dielectrophoresis, Proc. Natl. Acad. Sci. U. S. A 104 (2007) 20708–20712.

[19] a) K. Wang, P. Hampson, J. Hazeldine, V. Krystof, M. Strnad, et al., Cyclin-dependent kinase 9 activity regulates neutrophil spontaneous apoptosis, PLoS One 7 (2012), e30128;
b) V. Krystof, S. Baumli, R. Fürst, Perspective of cyclin-dependent kinase 9 (CDK9) as a drug target, Curr. Pharmaceut. Des. 18 (2012) 2883–2890.

[20] S.H. Chao, D.H. Price, Flavopiridol inactivates P-TEFb and blocks most RNA polymerase II transcription in vivo, J. Biol. Chem. 276 (2001) 31793–31799.

[21] a) A. Yokoyama, M. Lin, A. Naresh, I. Kitabayashi, M.L. Cleary, A higher-order complex containing AF4- and ENL-family proteins with P-TEFb facilitates oncogenic and physiologic MLL-dependent transcription, Canc. Cell 17 (2010) 198–212;
b) E.A. Bowman, W.G. Kelly, RNA polymerase II transcription elongation and Pol II CTD Ser2 phosphorylation: a tail of two kinases, Nucleus 5 (2014) 224–236.

[22] A.M. Narasimha, M. Kaulich, G.S. Shapiro, Y.J. Choi, P. Sicinski, S.F. Dowdy, Cyclin D activates the Rb tumor suppressor by mono-phosphorylation, Elife 3 (2014) 1–21.

[23] W.C. Burhans, M. Weinberger, M.A. Marchetti, L. Ramachandran, G. D'Urso, J.A. Huberman, Apoptosis-like yeast cell death in response to DNA damage and replication defects, (ROS) Mutat. Res. 532 (2003) 227–243.

[24] C.A. Davison, et al., Antioxidant enzymes mediate survival of breast cancer cells deprived of extracellular matrix, Canc. Res. 73 (2013) 3704–3715.

[25] MRuby-Mito-7 was obtained from Addgene plasmid # 55874 (a gift from Michael Davidson).

[26] a) S. Baumli, G. Lolli, E.D. Lowe, S. Troiani, L. Rusconi, A.N. Bullock, J.E. Debreczeni, S. Knapp, L.N. Johnson, The structure of P-TEFb (CDK9/cyclin T1), its complex with flavopiridol and regulation by phosphorylation, EMBO J. 27 (2008) 1907–1918;
b) N.R. Brown, M.E. Noble, J.A. Endicott, L.N. Johnson, The structural basis for specificity of substrate and recruitment peptides for cyclin-dependent kinases, Nat. Cell Biol. 1 (1999) 438.

[27] R.A. Friesner, R.B. Murphy, M.P. Repasky, L.L. Frye, J.R. Greenwood, T.A. Halgren, P.C. Sanschagrin, D.T. Mainz, Extra Precision Glide: docking and scoring incorporating a model of hydrophobic enclosure for protein-ligand complexes, J. Med. Chem. 49 (2006) 6177–6196.